Published in final edited form as:
Free Radic Biol Med. 2012 September 1; 53(5): 1139–1151. doi:10.1016/j.freeradbiomed.2012.06.012.

INCREASED NADPH OXIDASE DERIVED SUPEROXIDE IS INVOLVED IN THE NEURONAL CELL DEATH INDUCED BY HYPOXIA ISCHEMIA IN NEONATAL HIPPOCAMPAL SLICE CULTURES

Qing Lu[1], **Mark S. Wainwright**[2], **Valerie A. Harris**[1], **Saurabh Aggarwal**[1], **Yali Hou**[1], **Thomas Rau**[3], **David J. Poulsen**[3], and **Stephen M Black**[1]

[1]Vascular Biology Center, Georgia Health Sciences University, Augusta, GA 30912, USA

[2]Department of Pediatrics, Northwestern University Feinberg School of Medicine, Chicago, IL 60614

[3]Department of Biomedical and Pharmaceutical Sciences, University of Missoula, MT 59812, USA

Abstract

Neonatal brain hypoxia ischemia (HI) results in neuronal cell death. Previous studies indicate that reactive oxygen species (ROS) such as superoxide, play a key role in this process. However, the cellular sources have not been established. In this study we examined the role of the nicotinamide adenine dinucleotide phosphate (NADPH) oxidase complex in neonatal HI brain injury and elucidated its mechanism of activation. Rat hippocampal slices were exposed to oxygen glucose deprivation (OGD) to mimic the conditions seen in HI. Initial studies confirmed an important role for NADPH oxidase derived superoxide in the oxidative stress associated with OGD. Further, the OGD-mediated increase in apoptotic cell death was inhibited by the NADPH oxidase inhibitor, apocynin. The activation of NADPH oxidase was found to be dependent on the p38 mitogen-activated protein kinase mediated phosphorylation and activation of the $p47^{phox}$ subunit. Using an adeno-associated virus antisense construct to selectively decrease $p47^{phox}$ expression in neurons, and showed that this lead to inhibition both of the increase in superoxide and neuronal cell death associated with OGD. We also found that NADPH oxidase inhibition in a neonatal rat model of HI or scavenging hydrogen peroxide (H_2O_2) reduced brain injury. Thus, we conclude that activation of the NADPH oxidase complex contributes to the oxidative stress during HI and that therapies targeted against this complex could exhibit neuroprotection against the brain injury associated with neonatal HI.

Keywords

Hypoxia-ischemia; neuronal cell death; apoptosis; superoxide; Hydrogen peroxide; NADPH oxidase; $p47^{phox}$; p38MAP kinase; neonatal brain

Corresponding Author: Stephen M, Black, Ph.D. Georgia Health Sciences University, CB3211B Medical College of Georgia, Augusta, GA 30912, USA, sblack@georgiahealth.edu Phone: (706) 721-7860 Fax: (706) 721-9799.

INTRODUCTION

Neonatal hypoxia-ischemia (HI) remains an important cause of acute mortality and chronic morbidity in infants and children. The neurologic consequences of injury include mental retardation, epilepsy, cerebral palsy, and blindness [1]. It has been estimated that HI injury occurs in approximately 2–4 out of every 1000 full-term births in developed countries and is 20 to 30 times higher in developing countries [2, 3]. The mechanism of brain damage associated with HI is only partly understood. Evidence indicates that reactive oxygen (ROS) species such as superoxide are important mediators of ischemic neuronal death [4–6]. However, little is known regarding the specific cellular sources of these ROS.

Although neuronal superoxide production is widely attributed to mitochondria, neurons also express the nicotinamide adenine dinucleotide phosphate (NADPH) oxidase complex [7], a superoxide-generating enzyme first identified in phagocytes [8]. Superoxide produced by neuronal NADPH oxidase is thought to function in long-term potentiation and intercellular signaling [9] but increased levels of superoxide can also cause oxidative stress and neuronal cell death [10, 11]. NADPH oxidase is a transmembrane protein complex that transports electrons across biological membranes reducing oxygen to superoxide. The NADPH oxidase enzyme complex consists of the membrane bound $p22^{phox}$ and $gp91^{phox}$ subunits, several cytosolic proteins $p47^{phox}$, $p67^{phox}$, and $p40^{phox}$, and the G-protein, Rac1 [12]. NADPH oxidase is activated when the cytosolic subunits are phosphorylated, especially $p47^{phox}$, resulting in their translocation to the plasma membrane and formation of the active NADPH oxidase complex [12, 13]. The inhibition of NADPH oxidase may have benefit in stroke outcome, at least in adults [14].

The aim of the present study was to investigate the role of the NADPH oxidase complex in the oxidative stress associated with HI and its role in neonatal brain injury associated with HI. Using both an *in vitro* hippocampal slice culture model and an *in vivo* model of neonatal HI we analyzed $p47^{phox}$ expression, superoxide levels, infarct volume and neuronal cell death after OGD. Our data indicate that NADPH oxidase plays a major role in the increased superoxide generation associated with HI. Further, we found that $p47^{phox}$ translocation to the plasma membrane was dependent on p38MAP kinase signaling and that both pharmacologic inhibition and AAV-mediated neuronal specific expression of an antisense $p47^{phox}$ construct decreased the neuronal cell death associated with OGD in slice cultures. In the neonatal rat, HI was also associated with increased NADPH oxidase activity, superoxide generation and brain injury, while inhibition of NADPH oxidase reduced neurologic injury. Together our data suggest that therapies targeted against NADPH oxidase may have clinical utility in the treatment of perinatal asphyxia.

METHODS

Hippocampal Slice Culture and OGD exposure

Neonatal rats (Sprague-Dawley, Charles River, Wilmington, MA, USA) at postnatal Day 7 (P7) were decapitated and the hippocampi dissected under sterile conditions. Each hippocampus was sliced into 400μm slices using a Mcllwain tissue chopper (Science Products GmbH, Switzerland). Slices were then cultured on permeable membrane Millicell inserts (Millipore, Billerica, MA, USA) (0.4μm pore size) in six well plates for 6 days at 37°C in 5% CO_2. For the first two days, the slices were maintained in a primary plating medium: 50% Opti-Mem (Gibco, Grand Island, NY, USA), 25% HBSS, 25% heat inactivated horse serum, 5mg/ml D-glucose (Sigma, St. Louis, MO, USA), and 1.5% PenStrep/Fungizone (Gibco, Grand Island, NY, USA). The primary plating media was changed at 24h. After 48h, the slices were switched to Neurobasal–A media (Gibco, Grand Island, NY, USA), with 1mM Glutamax, 1% PenStrep/Fungizone (Gibco, Grand Island,

NY, USA), and 2% B27 (Gibco, Grand Island, NY, USA) supplemented with anti-oxidants for a further 2 days. Then, 24h before exposure to OGD the culture medium was changed to neurobasal-A and B27 supplement without antioxidants. Just prior to OGD, a sucrose balanced salt solution (SBSS) (120mM NaCl, 5mM KCl, 1.25mM NaH_2PO_4, 2mM $MgSO_4$, 2mM $CaCl_2$, 25mM $NaHCO_3$, 20mM HEPES, 25mM sucrose, pH of 7.3) was infused for 1 hour with 5%CO_2 and 10L/h nitrogen gas. The inserts were then transferred into deoxygenated SBSS and placed in a ProOxC system chamber with oxygen controller (BioSpherix, NY, USA) and exposed to 0.1% O_2, 5%CO_2, 94.4% nitrogen for 90min at 37°C. The slices were then returned to oxygenated serum-free neurobasal medium with B27 supplement. The NADPH oxidase inhibitor, apocynin (0–100μM, from Sigma St. Louis, MO, USA) or the p38MAP kinase inhibitor, SB203580 (50μM, Calbiochem, Gibbstown, NJ, USA) were dissolved in dimethyl sulphoxide (DMSO) and added to the medium 2h before OGD. Control experiments contained the equivalent amount of DMSO that did not exceed 0.2% (v/v). All protocols were approved by the Institutional Animal Care and Committee at Georgia Health Sciences University and the University of Montana.

Quantification of Slice Culture Cell Death

Propidium iodide (PI, 1μg/mL, Sigma, St. Louis, MO, USA) was added to the culture medium 24h prior to OGD. Slice cultures were then examined prior to OGD using an inverted fluorescence microscope (Olympus IX51, Olympus, Japan) using an excitation wavelength of 510 to 550nm and an emission wavelength of 590nm. Slices showing distinct PI intake were then excluded from further study. Slice culture images were obtained at baseline, and 4-, 8-, 24-h after OGD using a 10-bit monochrome fluorescence camera (HAMAMATSU Digital Camera C4742-95, Hamamatsu, Japan), and processed with Image-Pro Plus6.0 (Media Cybernetics, Maryland, USA). The exposure time was set at 200ms, using a 4× magnification to capture the entire slice. The evaluation of cell death was performed using a modification of the method of Cronberg *et al* [15]. The fluorescence intensity of the whole slice area, as well as CA1, CA3 and DG subregions was quantified with Image-Pro (Media Cybernetics, Silver Spring, MD, USA). Values were then presented as mean IOD fluorescence intensity.

LDH Cytotoxicity Assay

Cytotoxicity was evaluated by quantification of lactate dehydrogenase (LDH) using a Cytotoxicity Detection Kit (Roche Applied Science, Mannheim, Germany) in the slice culture medium. Samples were analyzed at 0-, 4-, 8-, and 24-h after OGD. All LDH measurements were divided by their protein levels (Bradford protein assay, Bio-Rad Laboratories, CA, USA) to normalize for possible variability in tissue levels between inserts. Data was then presented as LDH absorbance divided by μg protein.

Histologic Evaluations

Slice cultures were washed in PBS, fixed in 4% paraformaldehyde (RT, 1h), then in 30% sucrose (RT, 1h), embedded in O.C.T embedding medium (Tissue-Tek, Sakura Finetechnical, Tokyo, Japan) and stored at −80°C overnight. Embedded slices were sectioned to 15μm thickness and each cryosection mounted on slides and stored in −80°C until used. Sections were analyzed for the presence of apoptotic nuclei using the DeadEnd Fluorometric TUNEL System (Promega, Madison, WI, USA). The DNA breaks were labeled with fluorescein-12-dUTP (green) and the nuclei stained using PI (red). Sections were examined by fluorescence microscopy using a standard fluorescein filter set to view the green fluorescence of fluorescein at 520nm while the fluorescence of PI was as described above. The average fluorescent intensities (to correct for differences in cell number) were quantified using ImagePro Plus v.5.0 imaging software (Media Cybernetics,

Silver Spring, MD, USA). Quantification of the TUNEL stained nuclei and total nuclei was processed by Image-Pro software and presented as a percentage of total nuclei in the field.

Plasma Membrane Isolation

The plasma membrane was isolated using the Pierce Mem-PER Eukaryotic Membrane Protein Extraction Reagent Kit according to manufacturer's protocol (Thermo Fisher Scientific, Rockford, IL, USA). Briefly, slice culture homogenate were pelleted by centrifugation and lyzed. The supernatant obtained by centrifugation at 10,000 *g* for 3 min was incubated at room temperature for 20 min. The tubes were then centrifuged at 10,000 *g* for 2 min, and the hydrophobic phase (bottom layer) separated from hydrophilic phase (top layer). The hydrophobic phase contains the plasma membrane fraction. The purity of the plasma membrane was demonstrated by probing with VDAC and Lamin B1 to identify mitochondrial or nuclear contamination respectively.

Immunoblot and Immunoprecipitation Analyses

After experimental treatment, slice cultures were washed with ice-cold phosphate-buffered saline, homogenized in lysis buffer containing 1% Triton X-100, 20 mM Tris, pH 7.4, 100 mM NaCl, with 1× protease inhibitor cocktail, and 1× phosphatase inhibitor cocktail (Sigma, St. Louis, MO, USA). Lysates were centrifuged at 13,000 *g* for 10min at 4°C to precipitate the debris, and the protein content in the supernatant determined by the Bio-Rad protein assay (Bio-Rad Laboratories, CA USA). Lysate protein (20μg/lane) was separated using 4–20% gradient gels (Thermo Scientific, Rockford, IL, USA) and transferred to PVDF membranes. The blots were the probed with the appropriate antibody overnight at 4°C. Primary antibodies used were anti-$p47^{phox}$, anti-p38 MAPK (sc-14015, sc-7972, Santa Cruz, CA, USA); anti Na^+K^+ ATPase (to normalize the membrane fractions, *ab8344*, Abcam Inc., Cambridge, MA, USA), anti β-actin mouse monoclonal (to normalize total protein, Sigma, St. Lousi, MO), anti-GAPDH mouse monoclonal (to normalize cytosolic protein, *ab8245*, Abcam Inc., Cambridge, MA, USA), anti-cleaved caspase 3 (Cell signaling, Danvers, MA, USA) and an anti-Rabbit GPx-1 we have previously developed [16]. Blots were washed in 1 × TBST (3 × 15min) and the appropriate secondary antibodies conjugated to HRP were then added for 1h at RT (Thermo Scientific, Rockford, IL, USA). After further washing in TBST (3 × 15min) bands were visualized by chemiluminescence (West-Femto, Pierce, Rockford, IL, USA) and quantified using a Kodak Molecular Imaging System (Kodak, Rochester, NY, USA).

For the immunoprecipitation assays, insoluble proteins were precipitated by centrifugation at 13,000g for 10 min at 4 °C, and the supernatants were then incubated overnight with an anti-$p47^{phox}$ or anti-p38MAKP antibody (2 μg) at 4 °C followed by incubation in protein G plus protein A–Sepharose (Calbiochem, Gibbstown, NJ, USA) for 2 h. The immune complexes were precipitated by centrifugation, washed three times with lysis buffer, boiled in SDS sample buffer, and subjected to SDS-PAGE on 4–12% polyacrylamide gels and transferred to a nitrocellulose membrane (Bio-Rad, Hercules, CA, USA). The membranes were blocked with 2% BSA in Tris-buffered saline containing 0.1% Tween, then incubated with anti-phosphoserine (Cat#05-1000, Millipore, Billerica, MA, USA) or anti-$p47^{phox}$ overnight at 4°C. After washing, the membranes were probed with horseradish peroxidase-conjugated goat antiserum to rabbit (W4011, Promega, Madison, WI, USA). Protein bands were visualized by exposing the membrane to Supersignal West Femto Maximum Sensitivity Substrate (Pierce, Rockford, IL, USA) and quantified using a Kodak Image Station 440 (Carestream Health, Inc. Rochester, NY, USA).

Measurement of Superoxide Levels using electron paramagnetic resonance (EPR) spectroscopy

Superoxide production was measured using EPR as we have previously described [17]. *In vitro*, hippocampal slices were homogenized in EPR buffer (7.5μM desferrioxamine, 25μM diethyldithiocarbamate, in 1× phosphate buffer saline) on ice. *In vivo*, rat pups were decapitated, the brain swiftly removed, chilled on an ice block and the hippocampi dissected (less than 5 minutes / pup). The hippocampi were then frozen on dry ice, and stored at −80°C until EPR analysis. The contralateral (left) hippocampi of each rat pup served as an internal hemispheric control for the hypoxicischemic ipsilateral (right) hippocampi. Pooled samples of 3 to 4 ipsilateral or contralateral hippocampi (0.075– 0.1g) were pulverized and immediately immersed in desferrioxamine and DETC chelated EPR buffer [DPBS supplemented with 25μM desferrioxamine (EMD Biosciences, Gibbstown, NJ, USA), 7.5mM diethythiocarbamate (Sigma, St. Louis, MO, USA). Homogenate protein levels were determined by Bradford analysis (ThermoScientific, Rockford, IL, USA) and adjusted to the same protein concentrations using spin trap stock solution of 25mg/ml 1-hydroxy-3-methoxycarbonyl-2,2,5,5-tetramethylpyrrolidine·HCl (CMH, Alexis Biochemicals, San Diego, CA, USA) in EPR buffer, 1/5 (v/v) final CMH concentration, and incubated on ice for 1 hour. Thirty five-μl aliquots of each incubated homogenate were then added to a 50μl capillary tube and analyzed using a MiniScope MS200 EPR (Magnettech, Berlin, Germany) at a microwave power of 40 mW, modulation amplitude of 3,000 mG, and modulation frequency of 100 kHz. EPR spectra were analyzed by measurement of amplitude using ANALYSIS software (version 2.02). To quantify the amount of superoxide generated, waveform amplitudes were normalized to those generated by xanthine-xanthine oxidase. A standard reaction of xanthine oxidase in the presence of xanthine and CMH was performed. A reaction curve was generated by adding 1 U/ml xanthine oxidase (0.5U/mg; Sigma, St. Louis, MO, USA) into 10μM xanthine (Sigma, St. Louis, MO, USA) solution in PBS, pH 7.4, in the EPR reaction buffer, described above. Reactions were allowed to proceed at 25°C for 60 minutes. Aliquots were taken from the reaction mixture at 5 min intervals and EPR spectra were analyzed as described above. Under standard reaction conditions, 1 unit of xanthine oxidase, converts 1 μmol of xanthine per minute at 25°C. From the resulting standard based curve, a coefficient of 303.6 EPR amplitude units/μmol of superoxide was produced in our reaction. The waveform amplitudes generated in tissue were then converted into nanomoles of superoxide per milligram/minute of protein utilizing this value. Initial studies also indicated that freezing samples did no alter relative changes between study groups although total levels of superoxide detected were higher in fresh samples (Supplemental Figure 1).

Generation of antisense $p47^{phox}$ and GPX-1 adeno associated viruses (AAV)

Recombinant AAV1 was packaged in cultures of HEK 293T cells. Approximately 1.5×10^7 293T cells were seeded into 150cm dishes in complete DMEM (Cellgro, Manassas, VA, USA) supplemented with 10% fetal bovine serum, 1mM MEM sodium pyruvate, 0.1 mM MEM nonessential amino acids solution, and 0.05% Penicillin-Streptomycin (5,000 units/ml). Twenty four hours after seeding the medium was changed to culture media containing 5% fetal bovine serum and cells were transfected with three separate plasmids: Adeno helper plasmid (pFΔ6), AAV helper encoding serotype 1 (H21), and AAV transgene expression cassette containing a polylinker (null), the $p47^{phox}$ cDNA sequence in the antisense orientation, or a GPx-1 cDNA sequence all flanked by the AAV2 inverted terminal repeats. Plasmids were transfected into HEK293T cells using polyfect according to the manufacturers conditions (Qiagen, Valencia, CA). Cultures were incubated at 37°C, 5% CO_2 for 72h, harvested and pelleted by centrifugation. The pellet were resuspended in 10 mM Tris, pH 8.0 and chilled on ice. Cells were lysed by three repeated freeze-thaw cycles in a dry ice-ethanol bath followed by sonication and treatment with 50U benzonase (Novagen,

Darmstadt, Germany) and 0.5% sodium deoxycholate for 30 min at 37°C. Viruses were purified by density gradient centrifugation in iodixinol according to the method of Zolotukhin *et al* [18]. Purified virus preparations are concentrated and desalted in artificial CSF by centrifugation in Millipore Ultrafree 15 filter devices. The titer of each virus (genomic particles/ml) was determined by qRT-PCR using primers and a probe specific for the WPRE sequence.

Virus delivery to hippocampal slice cultures

Freshly harvested hippocampal slices cultures (9–12 slices in 1ml of media) were transduced with either AAV-SYN-1p47^{phox}AS or AAV-SYN-1null vector (as a control) using 1×10^{11}genomic particles for 1 hour at RT. During virus adsorption, a steady stream of sterilized O_2 was bubbled into the media. After 1 hour slices were placed on Millipore membranes and cultured at least for one week to allow significant down-regulation of p47^{phox} or GFP expression prior to exposure to OGD.

Intracerebroventricular viral injections

Postnatal day 1 rat pups were cryo-anesthetized on ice for 5–7 minutes and received a right hemispheric intracerebroventricular injection at the level of the middle hippocampal region (stereotaxic coordinates: 0.7 mm anterior, 1.9 mm lateral to the bregma at a depth of 1.5mm). Three microliters of artificial cerebrospinal fluid (0.15M NaCl, 2.75 μM KCl, 1.20 mM $CaCl_2$, 0.85 mM $MgCl_2$) and 0.4% Trypan Blue (Sigma, St. Louis, MO, USA) was delivered in the presence or absence of 2.5×10^{12} genomic particles of GPx-1 AAV. At postnatal day 8, rat pups were subjected to hypoxia ischemia, as described below, and allowed to recover for 2h for analysis of GPx-1 protein levels and activity.

Measurement of GPx activity in hippocampal tissue

The Glutathione Peroxidase Activity Kit (Enzo Lifesciences, Ann Arbor, MI) was used to measure GPx activity in fresh hippocampal tissue. Briefly, hippocampi were swiftly dissected at postnatal day 8, after transcardial tissue perfusion with 0.9% NaCl solution to remove blood cells, homogenized in 1 × Assay Buffer, and centrifuged at 10,000 × g for 20 minutes. The protein concentration of each supernatant was determined using the BCA assay reagent (Thermoscientific, Rockford, IL) and 40 μg was added to a reaction mixture of 1× assay buffer containing cumene hydroperoxide, NADPH, GSH reductase in a final volume of 200 μl. During the 10 min reaction time, the rate of NADPH oxidation was measured spectrophotometrically at 340nm. Activity calculations were based on the rate of the decrease in absorbance, defined as the amount of enzyme (one unit of glutathione peroxidase) that results in oxidation of 1 nmole of NADPH to $NADP^+$ per minute at 25°C and calculated in nMol/mg/min of hippocampal tissue.

Rat Model of Neonatal Hypoxia-Ischemia

Using the well established Levine procedure for hypoxia-ischemia [19] modified by Rice *et al* [20], Postnatal day 7, or day 8 for the GPx-1 over-expression studies, rat pups were anesthetized with isoflurane (4% for induction; 3% for maintenance), and 20% oxygen at 1L/min flow rate. For the duration of the study, a heated induction chamber and surgical bed, (Microflex EZ Anesthesia System, Euthanex, Palmer, PA, USA), were used to maintain core body temperature between 35–36°C. Rectal temperature was monitored continuously using a sensitive microprobe thermometer (Physitemp Instruments, Clifton, NJ, USA). The right common carotid artery was exposed, permanently occluded by electrical coagulation and incision sutured. Sham operated pups received vessel manipulation without occlusion. Immediately after surgery, pups were placed in a temperature controlled recovery chamber to recover for 15 minutes before returning to the dam for 1–2 hours. For induction of

hypoxia-ischemia, pups were placed in a custom made, plexiglas, multi-chambered hypoxia device (Jarrold Manufacturing, St.Louis, MO, USA). Chamber water bath temperature was maintained at 37°C and each chamber infused with a calibrated mixture of warm, humidified 8% oxygen/balance nitrogen for 2.5 hours at a flow rate of 100ml/min. Oxygen concentration was monitored (Mini-Ox3000 oxygen analyzer, MSA Medical Products, Pittsburgh, PA, USA) and core body temperature of pups maintained between 35–36 °C throughout duration of hypoxia. Sham pups were also placed in chamber with exposure to room air only. Immediately after hypoxia, pups were placed in a temperature regulated recovery chamber (36°C), and allowed 1–2 hours of recovery before returning to dam. Pups were euthanized and decapitated after 2- or 24-h reperfusion. The brains were quickly removed for further experiments.

In vivo NADPH oxidase inhibition

An *in vivo* NAPPH oxidase inhibitor [21], gp91 dstat and its inactive analogue, scrambled gp91 ds-tat were commercially synthesized with a nine amino acid sequence coupled to an HIV viral coat “tat” moiety (Biosynthesis Inc., Lewisville, Texas) to allow cell penetration. When internalized, it antagonizes the docking of the cytosolic NADPH (nicotinamide adenine dinucleotide phosphate) oxidase subunit to its transmembrane component $gp91^{phox}$. Day one of dam delivery was designated postnatal day 0 (PN0). On postnatal day 6 (PN6), 24h before surgery, randomly sexed littermates (13–16gm body weight) were randomly assigned to receive vehicle, gp91 ds-tat or scrambled gp91 ds-tat peptide. The peptides were diluted in physiological saline and intraperitoneally injected at a dose of 25mg/kg. Vehicle groups received an equivalent injection volume of saline. The following day of surgery, PN7, intraperitoneal injections, as described above, were also administered during the post surgical recovery period, 30 min before the induction of hypoxia-ischemia.

Assessment of brain injury

The removed brains were placed in chilled PBS for 5 minutes before using a rodent neonatal matrix (Zivic Instruments, Pittsburgh, PA, USA) to make five 2 mm thick coronal sections. Sections from rostral tip to caudal end, were immersed in 2% TTC (2,3,5-triphenyl-tetrazolium) (Sigma, St.Louis, MO, USA) dissolved in 0.15M PBS, incubated for 20 minutes at room temperature followed by two five minute incubating rinses in PBS on ice, subsequent fixation in 10% formalin buffer and storage at 4°C, protected from light [22] Infarct injury was assessed within 7 days after staining. By indirect morphometric analysis [23], extent of infarct injury was determined. Stained sections were scanned, and digitized for infarct area using a flatbed scanner (HP Scanjet, HP, Omaha, NE, USA) and Scion Image Software (Scion, MD, USA). Infarct volumes were calculated by adding the sum of all areas for coronal sections multiplied by thickness. To account for post ischemic edema total ipsilateral infarct volume were calculated as the difference between total uninjured contralateral hemispheric volume minus uninfarcted ipsilateral tissue volume [24].

NADPH oxidase activity

Vehicle, SCR TAT $gp91^{phox}$ and TAT $gp91^{phox}$ treated right hippocampal tissue were collected and homogenated with Tris-sucrose buffer (10mM Tris base (Fisher, Pittsburgh, PA, USA), 340mM sucrose (Mallinkrodt Baker, Inc Philipsburg, NJ, USA), 1mM EDTA (Mallinkrodt Baker, Inc Philipsburg, NJ, USA), 10ug/ml protease inhibitor mixture (Sigma, St. Louis, MO, USA). The homogenate protein concentration was measured. NADPH oxidase activity was measured by a luminescence assay in the reaction buffer with 5μM Lucigenin, 1mM EGTA and 50mM phosphate buffer, pH 7.0. 100μg of homogenate protein + 100μM NADPH as substrate (Sigma, St. Louis, MO, USA) were added to 8mm test tube with 500 μl reaction buffer, then incubated at 37°C for 5 min. Photon emission was

measured at 15 seconds in a luminometer (model TD-20/20, Turner Designs, Sunnyvale, CA, USA).

In vivo Detection of superoxide using dihydroethidium (DHE) oxidation

To estimate changes in superoxide formation in the brain *in vivo*, dihydroethidine (DHE, Anaspec, Freemont, CA) was administered as described previously [25, 26]. Briefly, DHE was dissolved in DMSO to make a stock solution of 500 mg/ml, and further diluted to 5 mg/ml in saline [27]. Three groups of rat pups (vehicle, gp91-tat and scrambled gp91-tat treated) were injected intraperitoneally with DHE (50 mg/kg) before being placed in the hypoxic chamber as described above. After exposure to HI, the rats were sacrificed their brains were removed and sectioned (15μM). Cryosections were then evaluated for ethidium fluorescence using excitation at 488 nm and emission at 590 nm. Fluorescent intensities were quantified with Image-Pro (Media Cybernetics, Silver Spring, MD, USA). Values were then presented as mean IOD fluorescence intensity.

In vivo measurement of H_2O_2 levels

The Amplex Red Reagent (Molecular Probes) was used to detect H_2O_2 levels in fresh hippocampal slice cultures obtained from rats subjected to OGD and in snap-frozen rat hippocampal tissues exposed to hypoxia/ischemia in the presence or absence of intra-cerebro-ventricular transduction of GPx-1 AAV. Briefly, an equal amount (~10mg/sample) of rat hippocampal slice culture or tissue was incubated at room temperature for 30 min in master mix solution containing Amplex Red Reagent, horseradish peroxidase, and a buffer solution, according to the manufacturer's protocol. The supernatant was then collected by brief centrifugation, added to a black 96 well plate, and the fluorescence was read spectrophotometrically at excitation/emission 530/590nm. The concentration of H_2O_2 was determined through extrapolation from a standard curve. The fluorescent signal was normalized by protein concentration and reported as nM/min/μg protein.

Statistical Analysis

Statistical calculations were performed using the GraphPad Prism V. 4.01 software. The mean ± SD (Figures 9 & 10) or SE (Figures 1–8) were calculated for all samples, and significance was determined by either the Student's *t*-test or ANOVA with the Newman-Keuls or Bonferroni post hoc test. A value of $P < 0.05$ was considered significant.

RESULTS

OGD increases $p47^{phox}$ protein levels and membrane translocation in rat hippocampal slice cultures

Utilizing Western blot analysis, we initially determined if OGD altered $p47^{phox}$ protein levels. Our data indicate that OGD significantly increased $p47^{phox}$ protein levels (Fig. 1 A) and this increase was attenuated in the presence of ≥100μM of the NADPH oxidase inhibitor, apocynin (Fig. 1 A). In fact at higher doses (≥100μM) $p47^{phox}$ levels were reduced to below control levels (Fig. 1 A). Further, the increases in $p47^{phox}$ protein corresponded to an increase in its activation, as determined by an increase in its translocation to the plasma membrane (Fig. 1 B & C). Again apocynin (100μM) significantly reduced the membrane translocation of $p47^{phox}$ (Fig. 1 B & C).

OGD increases NADPH oxidase derived superoxide generation in rat hippocampal slice cultures

To determine if OGD increases oxidative stress in the hippocampal slice cultures, we utilized EPR spectroscopy and spin trapping to detect superoxide generation. We confirmed

that superoxide was significant increased after OGD (Fig. 2). This generation of superoxide was blocked when the slices were pretreated with the NADPH oxidase inhibitor, apocynin (Fig. 2).

NADPH oxidase inhibition attenuates the neuronal cell death associated with OGD in rat hippocampal slice cultures

To examine cell death in the slice cultures after OGD we quantified the mean fluorescence intensity (MFI) of PI uptake. PI uptake in whole hippocampal slice as well as the hippocampal subregions (CA1 CA3 and DG) were evaluated for 24h after OGD. Our data indicate that OGD caused a time dependent increase in PI uptake, indicative of increased cell damage (Fig. 3 A). The severity of cell death in CA3 region was significantly lower than CA1 and DG regions (Fig. 3 B). The NADPH oxidase inhibitor, apocynin, decreased PI uptake in the whole slice as well as the CA1 and DG regions but not in the CA3 region (Fig. 3 B). In addition, we measured lactate dehydrogenase (LDH) release into the slice cultures medium. After OGD exposure an increase in LDH release was observed (Fig. 3 C). Apocynin pretreatment significantly decreased LDH release into the culture medium (Fig. 3 C).

NADPH oxidase inhibition attenuates the neuronal apoptosis associated with OGD in rat hippocampal slice cultures

To further evaluate the effect of NADPH oxidase inhibition on the neuronal cell death associated with OGD we next evaluated markers of apoptosis. Our data demonstrated that OGD increased the levels of cleaved caspase 3 (Fig. 4 A) and this increase was prevented by pre-treatment with apocynin (Fig. 4 A). Further, we found that the OGD-mediated increase in TUNEL positive nuclei in the CA1 region (Fig. 4 B) was also significantly reduced by apocynin (Fig. 4 C).

AAV-mediated $p47^{phox}$ gene knockdown attenuates the neuronal cell death associated with OGD in rat hippocampal slice cultures

Pharmacologic inhibition always has the potential for unappreciated off-target effects. In addition, our analyses could not determine if the increases in NADPH oxidase activation were specific to neurons in the mixed cell population present in our slice cultures. Thus, we followed up our apocynin studies with a molecular analysis targeted at $p47^{phox}$. To accomplish this we utilized an AAV delivery system using the neuronal specific promoter, SYN 1 to specifically express an anti-sense construct of $p47^{phox}$ in neurons. Our initial studies indicated that the AAV-SYN-1$p47^{phox}$AS construct significantly reduced the levels of $p47^{phox}$ protein both in the presence and absence of OGD (Fig. 5 A & B). This correlated with a significant decrease in superoxide generation in response to OGD (Fig. 5 C & D). Further, we found that the AAV-SYN-1$p47^{phox}$AS construct significantly decreased both the PI uptake in the slice cultures (Fig. 6 A & B) and LDH release into the culture medium (Fig. 6 C). This decrease in neuronal cell death mediated by the knockdown of $p47^{phox}$ protein levels was also associated with a reduction in caspase 3 activation (Fig. 7 A & B) and the appearance of TUNEL positive nuclei (Fig. 7 C & D).

p38MAP kinase is responsible for the phosphorylation and plasma membrane translocation of $p47^{phox}$ in rat hippocampal slice cultures exposed to OGD

Our previous studies have indicated that the activation of p38MAP kinase signaling plays an important role in neuronal cell death associated OGD in rat hippocampal slice cultures [28]. Thus, we determined if this kinase lies upstream of $p47^{phox}$. Our data indicated that OGD increases the association of p38MAP kinase with $p47^{phox}$ (Fig. 8 A & B). Further, our data indicate that the inhibition of p38MAP kinase using SB203580 significantly reduced both

the OGD mediated translocation to the plasma membrane (Fig. 8 C & D) and the increase in $p47^{phox}$ phosphorylation (Fig. 8 E & F).

gp91ds-tat inhibits NADPH oxidase activity and reduces HI infarct volume and apoptosis in a rat model of neonatal hypoxia ischemia

We next determined whether NADPH oxidase activation was involved in the brain injury associated with HI in the neonatal rat. HI increased NADPH oxidase activity (Fig. 9 A). This increase in NADPH oxidase activity correlated with an increase in superoxide levels in the right hemisphere of the brain as estimated by EPR (Fig. 9 B) and DHE oxidation (Fig. 9 C & D). Further, gp91ds-tat, but not the scrambled control peptide, attenuated both the increase in NADPH oxidase activity (Fig. 9 A) and superoxide levels (Fig. 9 B–D). In addition, gp91ds-tat pre-treatment significantly reduced the infarct volume in the right hemisphere after OGD (Fig.10 A & B) and this correlated with a reduction in apoptosis (Fig. 10 C & D).

Scavenging H_2O_2 reduces HI infarct volume in a rat model of neonatal hypoxia ischemia

To determine if ROS downstream of superoxide were playing a role in the HI injury we measured H_2O_2 levels in hippocampal slice cultures exposed to OGD or in the hippocampus in the HI exposed neonatal rat. Our data indicate that H_2O_2 levels are increased by OGD in hippocampal slice cultures (Figure 11 A) while in the neonatal rat, Hi increases H_2O_2 levels in the right hippocampus (Fig. 11 B). To determine if the increases in H_2O_2 are involved in the neuronal injury associated with HI, we over-expressed GPx-1 using an AAV delivery system (AAV GPx-1). Two hours after HI, we found no reduction in the GPx-1 protein (Fig. 11 C) or GPx activity (Fig. 11 D) in the right hemisphere treated with aCSF. GPx-1 protein and GPx activity were significantly higher in the right hippocampus transduced with AAV GPx-1 (Fig. 11 C & D). The increase in GPx activity correlated with a significant reduction in H_2O_2 after HI (Fig. 11 B). Finally, GPx-1 over-expression significantly reduced the infarct volume in the right hemisphere after OGD (Fig.11 E & F).

DISCUSSION

Accumulating evidence from clinical and experimental studies indicates much of the neuronal injury associated with HI involves increased oxidative stress. The neonatal brain is highly susceptible to reactive oxygen species (ROS) induced damage due to high concentrations of lipids that are susceptible to peroxidation, low levels of protective antioxidants, high oxygen consumption, and high levels of free iron acting as prooxidants under pathological conditions [29]. Although ROS are recognized as a major player in HI brain injury, their cellular resources are still under resolved. In most cells, ROS can be produced from several sources, including the mitochondria, NADPH oxidases, cytochrome P450-based enzymes, xanthine oxidase and NO synthases. Among these, the NADPH oxidases appear to be the major source of ROS as they are the only enzyme dedicated to ROS generation [30]. Here, we advance the understanding of these processes by demonstrating both *in vitro* and *in vivo* that HI causes a dramatic increase in NADPH oxidase derived superoxide, that neurons are the source of this increase, and further identify a role for the p38 MAPK in the mechanisms by which translocation of $p47^{phox}$ leads to activation of NADPH and neurologic injury.

NADPH oxidase is a multi-subunit, membrane associated protein. It has two membrane-integrated subunits, $gp91^{phox}$ (NOX2) and $p22^{phox}$, namely cytochrome b558, as its catalytic core. The cytosolic subunits are $p40^{phox}$, $p47^{phox}$, $p67^{phox}$ and Rac. NOX2 is the electron transfer chain of the active NADPH oxidase with binding sites for FAD, NADPH and two hemes. $p47^{phox}$ is the organizer of the translocation, bringing $p67^{phox}$ into contact with

NOX2 while also recruiting $p40^{phox}$ into the complex. In agreement with this, our results showed $p47^{phox}$ translocation to the membrane was increased after OGD in both hippocampal slice cultures and the neonatal rat brain exposed to HI. Further, this membrane translocation correlated with elevated levels of superoxide, indicative of NADPH oxidase activation. The importance of $p47^{phox}$ in regulating NADPH oxidase activation has been demonstrated both in humans where $p47^{phox}$ deficiency leads to the development of chronic granulomatous disease, characterized by phagocytes unable to generate superoxide [31] while $p47^{phox}$ knockout mice exhibit a similar defect [32]. Cerebral aneurysm, another disease associated with increased ROS generation, is also markedly inhibited by $p47^{phox}$ deletion in mice [33] while we found that the NADPH oxidase inhibitor, apocynin decreased both the oxidative stress associated with OGD in rat hippocampal slice cultures and the resulting neuronal cell death. As apocynin, is known to inhibit NADPH oxidase activity by blocking the binding of $p47^{phox}$ to $gp91^{phox}$ these data confirm the key role of $p47^{phox}$ in the activation of NADPH oxidase in response to OGD. Several studies have recently shown a therapeutic benefit of apocynin in various neuronal injury models. For example, in mice, the infarcts induced by CK2 inhibition [34] or ischemia reperfusion [35] was attenuated by apocynin. Similarly, in a gerbil cerebral ischemia reperfusion injury model, apocynin decreased ROS production and hippocampal neuronal cell death [36].

As we also found using higher doses of apocynin, $p47^{phox}$ can be regulated through changes in its expression as has also been shown in the carotid body of rats exposed to chronic hypoxia [37]. However, the major form of regulation of $p47^{phox}$ is thought to be through the modulation of its phosphorylation status. Phosphorylation of $p47^{phox}$ leads to a conformational change in the protein that allows it to interact with $p22^{phox}$ and so initiate the formation of the active NADPH oxidase complex. The C-terminus proline-rich region of $p47^{phox}$ contains potential serine phosphorylation sites. Evidence from neutrophil studies using individual or combined mutations has shown that phosphorylated serines are necessary for $p47^{phox}$ activation. A number of kinases have been shown to be capable of phosphorylating $p47^{phox}$ including PKC [38–41] and mitogen-activated protein kinases [41–43]. We add to this by identifying p38MAP kinase (p38 MAPK) as another signaling pathway capable of activating NADPH oxidase through $p47^{phox}$ phosphorylation. p38 MAPK is a serine/threonine kinase belonging to the family of mitogen-activated protein kinases activated by phosphorylation of tyrosine and threonine residues. Studies have shown that p38 MAPK is activated in response to a number of inflammatory signals as well as ischemia-reperfusion injury [44, 45]. Recent evidence suggests that p38MAPK may be a therapeutic target in the CNS [46–48] and the p38 MAPK inhibitor, SB239063, has been shown to reduce the infarct volume and attenuate neurological deficits in a rat model of focal ischemic brain injury [49, 50]. Our previously published data also found that attenuating p38 MAPK signaling either pharmacologically or using an siRNA approach, reduced the neuronal cell death associated with OGD in rat hippocampal neurons [28]. Further, this correlated with a reduction in superoxide generation [28]. Our findings regarding a link between p38MAPK and $p47^{phox}$ phosphorylation is supported by studies in neutrophils where p38MAPK activation increased the phosphorylation of $p47^{phox}$ [51, 52] while p38MAPK inhibition blocked the translocation of $p47^{phox}$ to the plasma membrane [53]. Further analyses identified the phosphorylation site as Ser345 [54], and although our studies did not determine if the same site is phosphorylated, our immunoprecipitation data identified a direct interaction between $p47^{phox}$ and p38MAPK making it likely that the same serine residue is phosphorylated. The MAPK pathway is typically composed of a highly conserved MAPK module including three kinases, namely MAPK kinase kinase (MKKK), MAPK kinase (MKK), and MAPK. In our studies we have not identified the signaling pathway by which OGD or HI activate p38MAPK although prior studies have indicated that the upstream kinases MEKK4 (an MKKK) can activate MKK3, MKK4, or MKK6, which subsequently phosphorylate p38 MAPK at Thr180 and Tyr182 [55, 56]. In addition to its

activation by upstream kinases, a MKK-independent mechanism has been identified in which transforming growth factor- β-activated protein kinase 1 (TAK1)-binding protein interacts with p38MAPKα and induces its autophosphorylation [57]. Beyond MKKKs and MKKs, the further upstream activator of p38MAPK is complex and has not been clearly elucidated. It is well known that exposure of neurons to HI triggers excessive and pathological glutamate release, which causes Ca^{2+} overload. This influx of Ca^{2+} into cells can activate a variety of enzymes, producing a cascade of events that eventually leads to cell injury and death [58–60]. Ca^{2+}/camodulin-dependent protein kinase II (CaMKII) is one of the most abundant proteins in the central nervous system and plays important roles in many neuronal processes and the Ca^{2+} influx after HI stimulates CaMKII activity [61]. Studies have also identified a close relationship between CaMKII signaling and ROS production [62] and we have recently reported that CaMKII can cause the phosphorylation and activation of NADPH oxidase, leading to enhanced generation of superoxide [63]. Combined with the results in this study, we speculate that CaMKII might be the upstream regulator of p38MAPK in HI brain injury. However, further studies will be required to confirm this link.

We also found that a $gp91^{phox}$ docking sequence (ds) peptide that attenuates the interaction of $gp91^{phox}$ (NOX2) with $p47^{phox}$ [64] was able to inhibit NADPH oxidase mediated superoxide generation, apoptotic neuronal cell death, and infarct size in a neonatal rat model of HI. The efficacy of this peptide in inhibiting NADPH oxidase derived superoxide has been demonstrated in a number of model systems. However, it should be noted that the sequence contained in $gp91^{phox}$ds peptide is also conserved in NOX1 and NOX4. Thus, it may not be specific for NOX2 but could act as a NOX1, NOX2 and NOX4 inhibitor [65]. This may be important since although NOX2 has been reported to be localized and expressed in the hippocampal CA1 region [66] the two other $gp91^{phox}$ homologues NOX1[67] and NOX4 [68] have also been found expressed in the brain. The role of these NOX isoforms in the neuronal injury associated with HI may vary. Reports have shown that infarct size was markedly reduced in NOX2-deficient mice [14]. Similarly, cerebral infarction and neurological deficits in a rat cerebral ischemia model were accompanied by an elevation of $gp91^{phox}$ mRNA [69]. The $gp91^{phox}$ds-tat peptide markedly significantly increased the number of surviving neurons in the CA1 region after reperfusion and this correlated with a reduction in NADPH oxidase activation and superoxide production [70]. Conversely, NOX1 does not appear to contribute to infarct size, but instead may limit cortical infarct development following cerebral ischemia [71]. NOX4 has also been shown to be up-regulated during stroke [68]. NOX4 mRNA levels have also been shown to be up-regulated following ischemic insult [72] but its role in regulating infarct size is still unclear. Thus, although it is unclear why the CA1 is more vulnerable to HI than sub region CA3 or the dentate gyrus it is possible that differences in NOX isoform expression may contribute. Alternatively, differences in cellular homogeneity may also be involved [73, 74].

In conclusion, our results both from hippocampal slice cultures exposed to OGD and the neonatal rat exposed to HI demonstrate that NADPH oxidase mediated superoxide generation contributes significantly to neonatal HI brain injury. In addition, our data demonstrate the key role played by p38 MAPK and $p47^{phox}$ phosphorylation in the signaling pathway leading to NADPH oxidase activation. These findings suggest that NADPH oxidase plays a critical role in brain injury associated with neonatal HI and that inhibiting the activity of the NADPH oxidase complex may have potential therapeutic value.

Supplementary Material

Refer to Web version on PubMed Central for supplementary material.

Acknowledgments

This research was supported in part by grant HD039110 to SMB.

REFERENCES

1. Smith KE, Keeney S, Zhang L, Perez-Polo JR, Rassin DK. The association of early blood oxygenation with child development in preterm infants with acute respiratory disorders. International Journal of Developmental Neuroscience. 2008; 26:125–131. [PubMed: 17988819]
2. Glass HC, Ferriero DM. Treatment of hypoxic-ischemic encephalopathy in newborns. Curr Treat Options Neurol. 2007; 9:414–423. [PubMed: 18173941]
3. Perlman JM. Intervention strategies for neonatal hypoxic-ischemic cerebral injury. Clin Ther. 2006; 28:1353–1365. [PubMed: 17062309]
4. Lipton P. Ischemic cell death in brain neurons. Physiol Rev. 1999; 79:1431–1568. [PubMed: 10508238]
5. Martin LJ, Brambrink AM, Price AC, Kaiser A, Agnew DM, Ichord RN, Traystman RJ. Neuronal death in newborn striatum after hypoxia-ischemia is necrosis and evolves with oxidative stress. Neurobiol Dis. 2000; 7:169–191. [PubMed: 10860783]
6. Clarkson AN, Sutherland BA, Appleton I. The biology and pathology of hypoxia-ischemia: an update. Arch Immunol Ther Exp (Warsz). 2005; 53:213–225. [PubMed: 15995582]
7. Cheret C, Gervais A, Lelli A, Colin C, Amar L, Ravassard P, Mallet J, Cumano A, Krause KH, Mallat M. Neurotoxic activation of microglia is promoted by a nox1-dependent NADPH oxidase. J Neurosci. 2008; 28:12039–12051. [PubMed: 19005069]
8. Al-Hathlol K, Phillips S, Seshia MK, Casiro O, Alvaro RE, Rigatto H. Alveolar capillary dysplasia. Report of a case of prolonged life without extracorporeal membrane oxygenation (ECMO) and review of the literature. Early Hum Dev. 2000; 57:85–94. [PubMed: 10735455]
9. Zhang P, Hou M, Li Y, Xu X, Barsoum M, Chen Y, Bache RJ. NADPH oxidase contributes to coronary endothelial dysfunction in the failing heart. Am J Physiol Heart Circ Physiol. 2009; 296:H840–846. [PubMed: 19168727]
10. Suh SW, Shin BS, Ma H, Van Hoecke M, Brennan AM, Yenari MA, Swanson RA. Glucose and NADPH oxidase drive neuronal superoxide formation in stroke. Ann Neurol. 2008; 64:654–663. [PubMed: 19107988]
11. Brennan AM, Suh SW, Won SJ, Narasimhan P, Kauppinen TM, Lee H, Edling Y, Chan PH, Swanson RA. NADPH oxidase is the primary source of superoxide induced by NMDA receptor activation. Nat Neurosci. 2009; 12:857–863. [PubMed: 19503084]
12. Bedard K, Krause KH. The NOX family of ROS-generating NADPH oxidases: physiology and pathophysiology. Physiol Rev. 2007; 87:245–313. [PubMed: 17237347]
13. Johnson JL, Park JW, Benna JE, Faust LP, Inanami O, Babior BM. Activation of p47(PHOX), a cytosolic subunit of the leukocyte NADPH oxidase. Phosphorylation of ser-359 or ser-370 precedes phosphorylation at other sites and is required for activity. J Biol Chem. 1998; 273:35147–35152. [PubMed: 9857051]
14. Walder CE, Green SP, Darbonne WC, Mathias J, Rae J, Dinauer MC, Curnutte JT, Thomas GR. Ischemic stroke injury is reduced in mice lacking a functional NADPH oxidase. Stroke. 1997; 28:2252–2258. [PubMed: 9368573]
15. Cronberg T, Rytter A, Asztely F, Soder A, Wieloch T. Glucose but Not Lactate in Combination With Acidosis Aggravates Ischemic Neuronal Death In Vitro. Stroke. 2004; 35:753–757. [PubMed: 14963271]
16. Khan JY, Black SM. Developmental changes in murine brain antioxidant enzymes. Pediatr Res. 2003; 54:77–82. [PubMed: 12646716]
17. Lu Q, Rau TF, Harris V, Johnson M, Poulsen DJ, Black SM. Increased p38 mitogen-activated protein kinase signaling is involved in the oxidative stress associated with oxygen and glucose deprivation in neonatal hippocampal slice cultures. Eur J Neurosci. 2011; 34:1093–1101. [PubMed: 21939459]

18. Zolotukhin S, Byrne BJ, Mason E, Zolotukhin I, Potter M, Chesnut K, Summerford C, Samulski RJ, Muzyczka N. Recombinant adeno-associated virus purification using novel methods improves infectious titer and yield. Gene Ther. 1999; 6:973–985. [PubMed: 10455399]
19. Levine S. Anoxic-ischemic encephalopathy in rats. Am J Pathol. 1960; 36:1–17. [PubMed: 14416289]
20. Rice JE 3rd, Vannucci RC, Brierley JB. The influence of immaturity on hypoxic-ischemic brain damage in the rat. Ann Neurol. 1981; 9:131–141. [PubMed: 7235629]
21. Rey, e. a. Circ. Res. 2001; 89:408–414. [PubMed: 11532901]
22. Bederson JB, Pitts LH, Germano SM, Nishimura MC, Davis RL, Bartkowski HM. Evaluation of 2,3,5-triphenyltetrazolium chloride as a stain for detection and quantification of experimental cerebral infarction in rats. Stroke. 1986; 17:1304–1308. [PubMed: 2433817]
23. Swanson RA, Morton MT, Tsao-Wu G, Savalos RA, Davidson C, Sharp FR. A semiautomated method for measuring brain infarct volume. J Cereb Blood Flow Metab. 1990; 10:290–293. [PubMed: 1689322]
24. Lin TN, He YY, Wu G, Khan M, Hsu CY. Effect of brain edema on infarct volume in a focal cerebral ischemia model in rats. Stroke. 1993; 24:117–121. [PubMed: 8418534]
25. Quick KL, Dugan LL. Superoxide stress identifies neurons at risk in a model of ataxia-telangiectasia. Ann Neurol. 2001; 49:627–635. [PubMed: 11357953]
26. Hu D, Serrano F, Oury TD, Klann E. Aging-dependent alterations in synaptic plasticity and memory in mice that overexpress extracellular superoxide dismutase. J Neurosci. 2006; 26:3933–3941. [PubMed: 16611809]
27. Yu F, Sugawara T, Chan PH. Treatment with dihydroethidium reduces infarct size after transient focal cerebral ischemia in mice. Brain Res. 2003; 978:223–227. [PubMed: 12834917]
28. Lu Q, Rau T, Harris VA, Johnson M, Poulsen DJ, Black SM. Increased p38 mitogen-activated protein kinase signaling is involved in the oxidative stress associated with oxygen and glucose deprivation in neonatal hippocampal slice cultures. Eur. J. Neurosci. 2011 In Press.
29. Saeed SA, Shad KF, Saleem T, Javed F, Khan MU. Some new prospects in the understanding of the molecular basis of the pathogenesis of stroke. Exp Brain Res. 2007; 182:1–10. [PubMed: 17665180]
30. Opitz N, Drummond GR, Selemidis S, Meurer S, Schmidt HH. The 'A's and 'O's of NADPH oxidase regulation: a commentary on “Subcellular localization and function of alternatively spliced Noxo1 isoforms”. Free Radic Biol Med. 2007; 42:175–179. [PubMed: 17189823]
31. Meischl C, Roos D. The molecular basis of chronic granulomatous disease. Springer Semin Immunopathol. 1998; 19:417–434. [PubMed: 9618766]
32. Jackson SH, Gallin JI, Holland SM. The p47phox mouse knock-out model of chronic granulomatous disease. J Exp Med. 1995; 182:751–758. [PubMed: 7650482]
33. Aoki T, Nishimura M, Kataoka H, Ishibashi R, Nozaki K, Hashimoto N. Reactive oxygen species modulate growth of cerebral aneurysms: a study using the free radical scavenger edaravone and p47phox(−/−) mice. Lab Invest. 2009; 89:730–741. [PubMed: 19381132]
34. Kim GS, Jung JE, Niizuma K, Chan PH. CK2 is a novel negative regulator of NADPH oxidase and a neuroprotectant in mice after cerebral ischemia. J Neurosci. 2009; 29:14779–14789. [PubMed: 19940173]
35. Chen H, Song YS, Chan PH. Inhibition of NADPH oxidase is neuroprotective after ischemia-reperfusion. J Cereb Blood Flow Metab. 2009; 29:1262–1272. [PubMed: 19417757]
36. Wang Q, Tompkins KD, Simonyi A, Korthuis RJ, Sun AY, Sun GY. Apocynin protects against global cerebral ischemia-reperfusion-induced oxidative stress and injury in the gerbil hippocampus. Brain Res. 2006; 1090:182–189. [PubMed: 16650838]
37. He L, Liu X, Chen J, Dinger B, Stensaas L, Fidone S. Modulation of chronic hypoxia-induced chemoreceptor hypersensitivity by NADPH oxidase subunits in rat carotid body. J Appl Physiol. 108:1304–1310. [PubMed: 20185631]
38. Nauseef WM, Volpp BD, McCormick S, Leidal KG, Clark RA. Assembly of the neutrophil respiratory burst oxidase. Protein kinase C promotes cytoskeletal and membrane association of cytosolic oxidase components. J Biol Chem. 1991; 266:5911–5917. [PubMed: 1848559]

39. Dang PM, Fontayne A, Hakim J, El Benna J, Perianin A. Protein kinase C zeta phosphorylates a subset of selective sites of the NADPH oxidase component p47phox and participates in formyl peptide-mediated neutrophil respiratory burst. J Immunol. 2001; 166:1206–1213. [PubMed: 11145703]
40. Reeves EP, Dekker LV, Forbes LV, Wientjes FB, Grogan A, Pappin DJ, Segal AW. Direct interaction between p47phox and protein kinase C: evidence for targeting of protein kinase C by p47phox in neutrophils. Biochem J. 1999; 344(Pt 3):859–866. [PubMed: 10585874]
41. Yamamori T, Inanami O, Nagahata H, Cui Y, Kuwabara M. Roles of p38 MAPK, PKC and PI3-K in the signaling pathways of NADPH oxidase activation and phagocytosis in bovine polymorphonuclear leukocytes. FEBS Lett. 2000; 467:253–258. [PubMed: 10675549]
42. Brown GE, Stewart MQ, Bissonnette SA, Elia AE, Wilker E, Yaffe MB. Distinct ligand-dependent roles for p38 MAPK in priming and activation of the neutrophil NADPH oxidase. J Biol Chem. 2004; 279:27059–27068. [PubMed: 15102856]
43. Dewas C, Fay M, Gougerot-Pocidalo MA, El-Benna J. The mitogen-activated protein kinase extracellular signal-regulated kinase 1/2 pathway is involved in formyl-methionyl-leucyl-phenylalanine-induced p47phox phosphorylation in human neutrophils. J Immunol. 2000; 165:5238–5244. [PubMed: 11046057]
44. Fujimoto H, Ohno M, Ayabe S, Kobayashi H, Ishizaka N, Kimura H, Yoshida K, Nagai R. Carbon monoxide protects against cardiac ischemia--reperfusion injury in vivo via MAPK and Akt--eNOS pathways. Arterioscler Thromb Vasc Biol. 2004; 24:1848–1853. [PubMed: 15308554]
45. Amersi F, Shen XD, Anselmo D, Melinek J, Iyer S, Southard DJ, Katori M, Volk HD, Busuttil RW, Buelow R, Kupiec-Weglinski JW. Ex vivo exposure to carbon monoxide prevents hepatic ischemia/reperfusion injury through p38 MAP kinase pathway. Hepatology. 2002; 35:815–823. [PubMed: 11915027]
46. Barone FC, Irving EA, Ray AM, Lee JC, Kassis S, Kumar S, Badger AM, Legos JJ, Erhardt JA, Ohlstein EH, Hunter AJ, Harrison DC, Philpott K, Smith BR, Adams JL, Parsons AA. Inhibition of p38 mitogen-activated protein kinase provides neuroprotection in cerebral focal ischemia. Med Res Rev. 2001; 21:129–145. [PubMed: 11223862]
47. Borders AS, de Almeida L, Van Eldik LJ, Watterson DM. The p38alpha mitogen-activated protein kinase as a central nervous system drug discovery target. BMC Neurosci. 2008; 9(Suppl 2):S12. [PubMed: 19090985]
48. Sun A, Liu M, Nguyen XV, Bing G. P38 MAP kinase is activated at early stages in Alzheimer's disease brain. Exp Neurol. 2003; 183:394–405. [PubMed: 14552880]
49. Barone FC, Irving EA, Ray AM, Lee JC, Kassis S, Kumar S, Badger AM, White RF, McVey MJ, Legos JJ, Erhardt JA, Nelson AH, Ohlstein EH, Hunter AJ, Ward K, Smith BR, Adams JL, Parsons AA. SB 239063, a second-generation p38 mitogen-activated protein kinase inhibitor, reduces brain injury and neurological deficits in cerebral focal ischemia. J Pharmacol Exp Ther. 2001; 296:312–321. [PubMed: 11160612]
50. Legos JJ, Erhardt JA, White RF, Lenhard SC, Chandra S, Parsons AA, Tuma RF, Barone FC. SB 239063, a novel p38 inhibitor, attenuates early neuronal injury following ischemia. Brain Res. 2001; 892:70–77. [PubMed: 11172750]
51. El Benna J, Han J, Park JW, Schmid E, Ulevitch RJ, Babior BM. Activation of p38 in stimulated human neutrophils: phosphorylation of the oxidase component p47phox by p38 and ERK but not by JNK. Arch Biochem Biophys. 1996; 334:395–400. [PubMed: 8900416]
52. Manke IA, Nguyen A, Lim D, Stewart MQ, Elia AE, Yaffe MB. MAPKAP kinase-2 is a cell cycle checkpoint kinase that regulates the G2/M transition and S phase progression in response to UV irradiation. Mol Cell. 2005; 17:37–48. [PubMed: 15629715]
53. Yamamori T, Inanami O, Sumimoto H, Akasaki T, Nagahata H, Kuwabara M. Relationship between p38 mitogen-activated protein kinase and small GTPase Rac for the activation of NADPH oxidase in bovine neutrophils. Biochem Biophys Res Commun. 2002; 293:1571–1578. [PubMed: 12054696]
54. Dang PM, Stensballe A, Boussetta T, Raad H, Dewas C, Kroviarski Y, Hayem G, Jensen ON, Gougerot-Pocidalo MA, El-Benna J. A specific p47phox -serine phosphorylated by convergent MAPKs mediates neutrophil NADPH oxidase priming at inflammatory sites. J Clin Invest. 2006; 116:2033–2043. [PubMed: 16778989]

55. Raingeaud J, Whitmarsh AJ, Barrett T, Derijard B, Davis RJ. MKK3- and MKK6-regulated gene expression is mediated by the p38 mitogen-activated protein kinase signal transduction pathway. Mol Cell Biol. 1996; 16:1247–1255. [PubMed: 8622669]
56. Derijard B, Raingeaud J, Barrett T, Wu IH, Han J, Ulevitch RJ, Davis RJ. Independent human MAP-kinase signal transduction pathways defined by MEK and MKK isoforms. Science. 1995; 267:682–685. [PubMed: 7839144]
57. Ge B, Gram H, Di Padova F, Huang B, New L, Ulevitch RJ, Luo Y, Han J. MAPKK-independent activation of p38alpha mediated by TAB1-dependent autophosphorylation of p38alpha. Science. 2002; 295:1291–1294. [PubMed: 11847341]
58. Trump BF, Berezesky IK. Calcium-mediated cell injury and cell death. FASEB J. 1995; 9:219–228. [PubMed: 7781924]
59. Wojda U, Salinska E, Kuznicki J. Calcium ions in neuronal degeneration. IUBMB Life. 2008; 60:575–590. [PubMed: 18478527]
60. Kristian T, Siesjo BK. Calcium in ischemic cell death. Stroke. 1998; 29:705–718. [PubMed: 9506616]
61. Aronowski J, Grotta JC, Waxham MN. Ischemia-induced translocation of Ca2+/calmodulin-dependent protein kinase II: potential role in neuronal damage. J Neurochem. 1992; 58:1743–1753. [PubMed: 1313852]
62. Kelly EK, Wang L, Ivashkiv LB. Calcium-activated pathways and oxidative burst mediate zymosan-induced signaling and IL-10 production in human macrophages. J Immunol. 2010; 184:5545–5552. [PubMed: 20400701]
63. Pandey D, Gratton JP, Rafikov R, Black SM, Fulton DJ. Calcium/calmodulin-dependent kinase II mediates the phosphorylation and activation of NADPH oxidase 5. Mol Pharmacol. 2011; 80:407–415. [PubMed: 21642394]
64. Rey FE, Cifuentes ME, Kiarash A, Quinn MT, Pagano PJ. Novel competitive inhibitor of NAD(P)H oxidase assembly attenuates vascular O(2)(−) and systolic blood pressure in mice. Circ. Res. 2001; 89:408–414. [PubMed: 11532901]
65. Arnold RS, Shi J, Murad E, Whalen AM, Sun CQ, Polavarapu R, Parthasarathy S, Petros JA, Lambeth JD. Hydrogen peroxide mediates the cell growth and transformation caused by the mitogenic oxidase Nox1. Proc Natl Acad Sci U S A. 2001; 98:5550–5555. [PubMed: 11331784]
66. Serrano F, Kolluri NS, Wientjes FB, Card JP, Klann E. NADPH oxidase immunoreactivity in the mouse brain. Brain Res. 2003; 988:193–198. [PubMed: 14519542]
67. Ibi M, Katsuyama M, Fan C, Iwata K, Nishinaka T, Yokoyama T, Yabe-Nishimura C. NOX1/NADPH oxidase negatively regulates nerve growth factor-induced neurite outgrowth. Free Radic Biol Med. 2006; 40:1785–1795. [PubMed: 16678016]
68. Vallet P, Charnay Y, Steger K, Ogier-Denis E, Kovari E, Herrmann F, Michel JP, Szanto I. Neuronal expression of the NADPH oxidase NOX4, and its regulation in mouse experimental brain ischemia. Neuroscience. 2005; 132:233–238. [PubMed: 15802177]
69. Kusaka I, Kusaka G, Zhou C, Ishikawa M, Nanda A, Granger DN, Zhang JH, Tang J. Role of AT1 receptors and NAD(P)H oxidase in diabetes-aggravated ischemic brain injury. Am J Physiol Heart Circ Physiol. 2004; 286:H2442–2451. [PubMed: 15148062]
70. Zhang QG, Raz L, Wang R, Han D, De Sevilla L, Yang F, Vadlamudi RK, Brann DW. Estrogen attenuates ischemic oxidative damage via an estrogen receptor alpha-mediated inhibition of NADPH oxidase activation. J Neurosci. 2009; 29:13823–13836. [PubMed: 19889994]
71. Jackman KA, Miller AA, Drummond GR, Sobey CG. Importance of NOX1 for angiotensin II-induced cerebrovascular superoxide production and cortical infarct volume following ischemic stroke. Brain Res. 2009; 1286:215–220. [PubMed: 19559686]
72. Serrander L, Cartier L, Bedard K, Banfi B, Lardy B, Plastre O, Sienkiewicz A, Forro L, Schlegel W, Krause KH. NOX4 activity is determined by mRNA levels and reveals a unique pattern of ROS generation. Biochem J. 2007; 406:105–114. [PubMed: 17501721]
73. Shiino A, Matsuda M, Handa J, Chance B. Poor recovery of mitochondrial redox state in CA1 after transient forebrain ischemia in gerbils. Stroke; a journal of cerebral circulation. 1998; 29:2421–2424. discussion 2425.

74. Newrzella D, Pahlavan PS, Kruger C, Boehm C, Sorgenfrei O, Schrock H, Eisenhardt G, Bischoff N, Vogt G, Wafzig O, Rossner M, Maurer MH, Hiemisch H, Bach A, Kuschinsky W, Schneider A. The functional genome of CA1 and CA3 neurons under native conditions and in response to ischemia. BMC Genomics. 2007; 8:370. [PubMed: 17937787]

- Hypoxia-ischemia stimulates superoxide generation via NADPH oxidase.
- NADPH oxidase activation occurs via the phosphorylation of $p47^{phox}$ by p38MAPK.
- The toxic metabolite inducing neuronal injury appears to be hydrogen peroxide.
- Reducing reactive oxygen species attenuates the neuronal injury associated with HI.

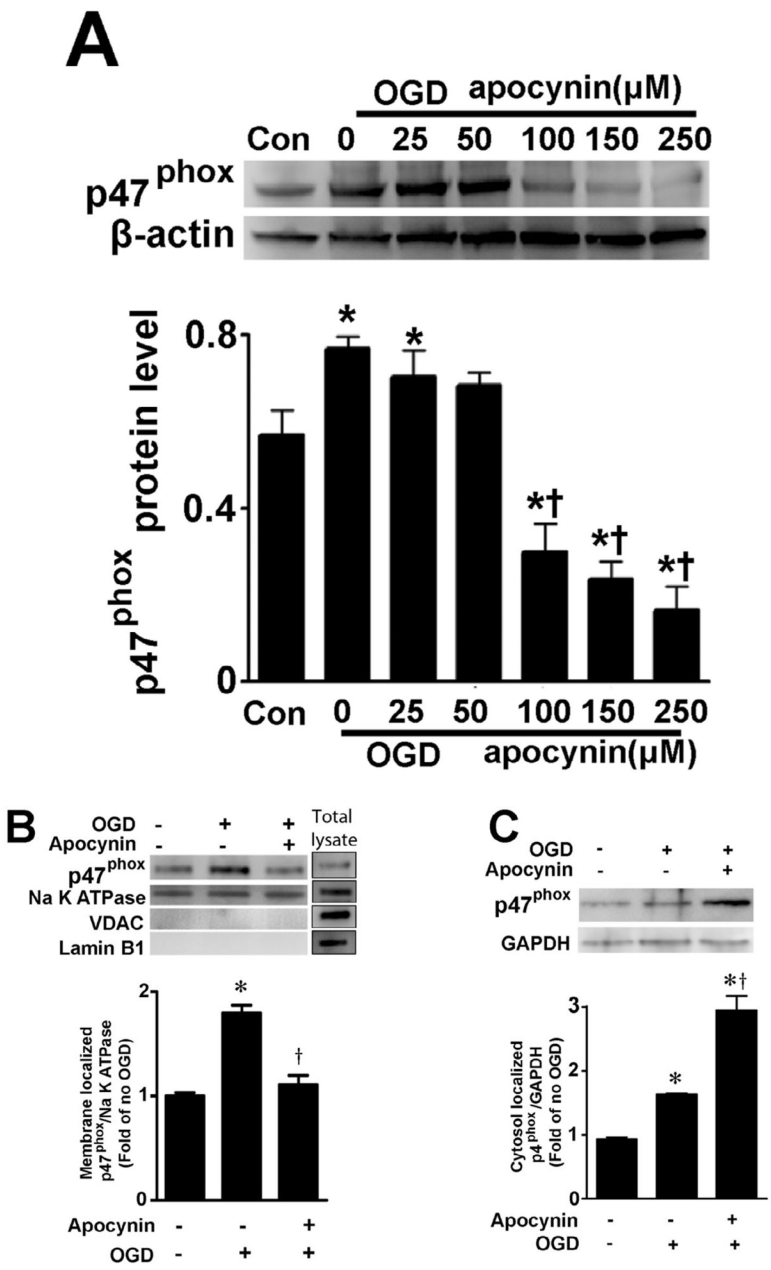

Figure 1. Oxygen glucose deprivation increases p47^{phox} protein levels in rat hippocampal slice cultures

Rat hippocampal slice cultures were exposed to OGD in the presence or absence of the NADPH oxidase inhibitor, apocynin (0–250μM, 2h prior to OGD). Slices were harvested 8h after OGD and subjected to Western blot analysis to determine effects on total p47^{phox} protein levels. A representative blot is shown (A). Protein loading was normalized by reprobing with β-actin and the data plotted as the ratio of p47^{phox}:β-actin. In addition the affect of OGD on membrane (B) and cytosolic (C) localized p47^{phox} was determined. Again representative images are shown. Loading of the membrane fraction was normalized by reprobing with NaK ATPase and the data plotted as the ratio of p47^{phox}: NaK ATPase normalized to 1.0 for the control. Similarly, loading of the cytosolic fraction was normalized by reprobing with GAPDH and the data plotted as the ratio of p47^{phox}: GAPDH normalized

to 1.0 for the control. Data are presented as mean ± S.E from 4 independent experiments using 24 pooled slices per experiment. * $P<0.05$ vs. control, † $P<0.05$ vs. OGD alone.

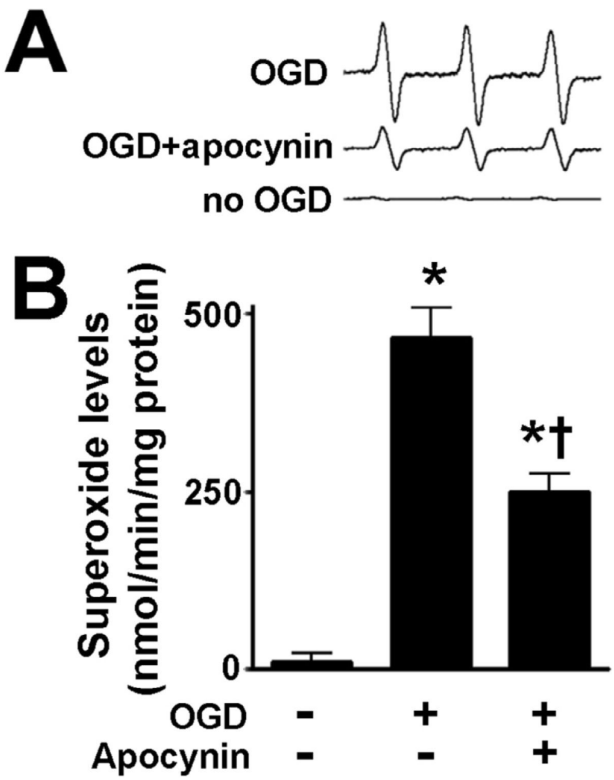

Figure 2. NADPH oxidase inhibition attenuates superoxide generation in rat hippocampal slice cultures exposed to oxygen glucose deprivation

Rat hippocampal slice cultures were exposed to OGD in the presence or absence of the NADPH oxidase inhibitor, apocynin (100μM, 2h prior to OGD) then harvested at 8h then subjected to electron paramagnetic resonance (EPR) using the spin-trap compound 1-hydroxy-3-methoxycarbonyl-2,2,5,5-tetramethylpyrrolidine HCl (CMH) to determine superoxide levels. Representative EPR waveforms are shown (A). Absolute levels of superoxide generation were then determined as nmols superoxide generated/min/mg protein (B). Apocynin attenuates the OGD-mediated increase in superoxide levels. Values are presented as mean ± S.E from 4 independent experiments using 24 pooled slices per experiment. * $P<0.05$ vs. no OGD, † $P<0.05$ vs. OGD alone.

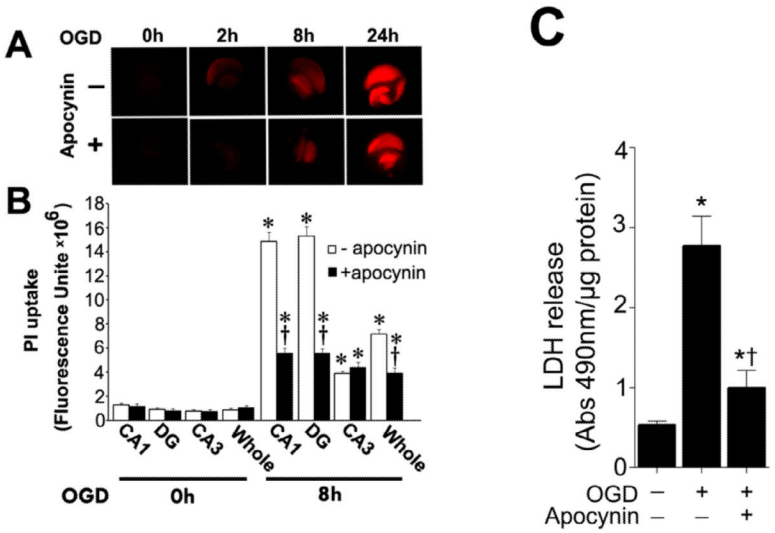

Figure. 3. Apocynin attenuates oxygen glucose deprivation mediated regional cell injury in rat hippocampal slice cultures

Rat hippocampal slice cultures were exposed to OGD in the presence or absence of the NADPH oxidase inhibitor, apocynin (100μM, 2h prior to OGD). The effect on cell injury was then quantified by measuring changes in PI uptake fluorescence either in the whole slice, CA1, CA3, or DG subregions 8h after OGD. Representative images are shown for the PI uptake in the entire slice (A). PI uptake in the whole slice exhibited a time-dependent increase and apocynin pretreatment significantly decreased PI uptake (B). Similar effects were found in the CA1 (B) and DG sub-region (B). However, in the CA3 area apocynin pretreatment did not show a significant decrease in PI uptake (B). In addition, LDH release from the slice cultures was also determined (C). The LDH absorbance at 490nm was divided by protein content. Data are presented as mean ± S.E. from 4 independent experiments. * $P<0.05$ vs. no OGD, † $P<0.05$ vs. OGD alone.

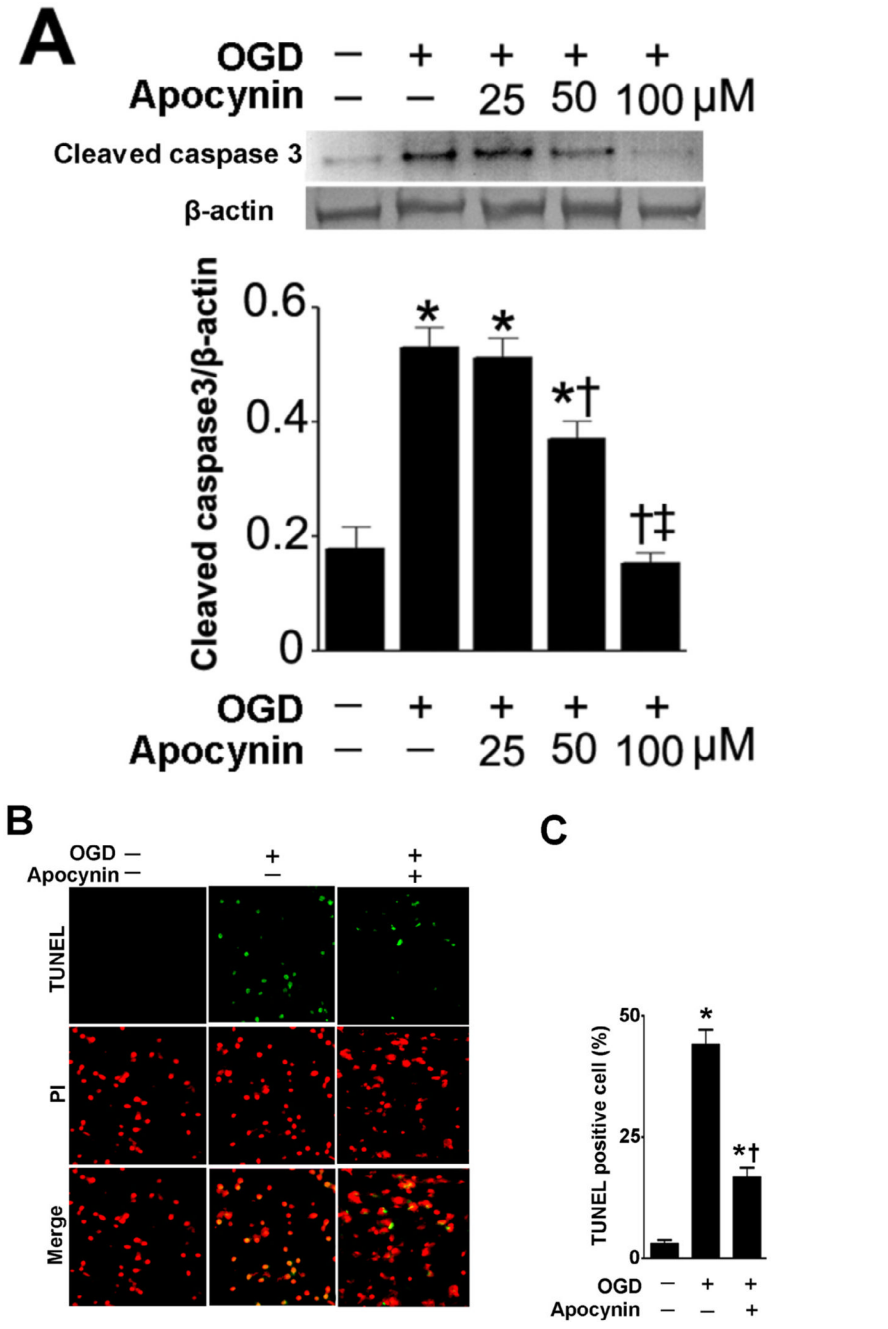

Figure 4. NADPH oxidase inhibition attenuates apoptosis in rat hippocampal slice cultures exposed to oxygen glucose deprivation

Rat hippocampal slice cultures were exposed to OGD in the presence or absence of the NADPH oxidase inhibitor, apocynin (0–100μM, 2h prior to OGD). Slices were harvested 8h after OGD and subjected to Western blot analysis to determine effects on cleaved caspase-3 (A). A representative blot is shown (A). OGD increases cleaved caspase-3 levels and this is attenuated by apocynin pretreatment at 50- and 100-μM (A). Slices were also subjected to TUNEL analysis. Representative images are shown demonstrating the TUNEL staining of apoptotic cells (green) co-localized with PI staining of all the nuclei (red) resulted in more yellow (merged) nuclei than in apocynin pretreated slices (B). The magnification used was

10×. Quantification of the percentage of apoptotic nuclei to total nuclei was also carried out indicating that apocynin decreased the level of apoptotic nuclei in response to OGD (C). Data are presented as mean ± S.E from 4 independent experiments using 24 pooled slices per experiment. * $P<0.05$ vs. no OGD, † $P<0.05$ vs.

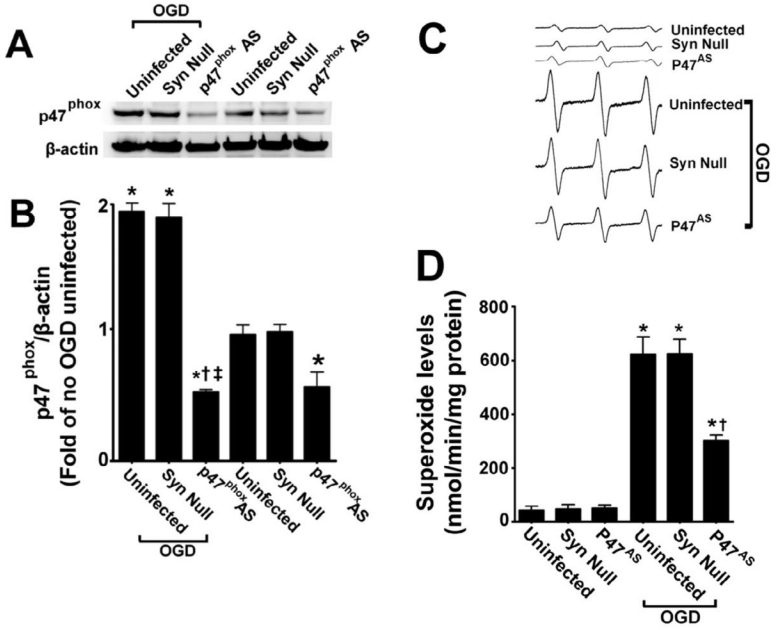

Figure 5. Targeted decreases in p47^{phox} expression in neuronal cells attenuates superoxide generation in rat hippocampal slice cultures

Rat hippocampal slice cultures were transduced with the AAV-SYN-1-p47^{phox}AS, an AAV-SYN-1null construct, or were untransduced. After 7 days slices were exposed or not to OGD, harvested 8h later then subjected to Western blot analysis to determine effects on p47^{phox} protein levels. A representative image is shown (A). The AAV-SYN-1-p47^{phox}AS construct significantly decreases p47^{phox} levels in control slices (B) and prevents the increase in p47^{phox} protein levels in response to OGD (B). Slices were also subjected to electron paramagnetic resonance (EPR) using the spin-trap compound 1-hydroxy-3-methoxycarbonyl-2,2,5,5-tetramethylpyrrolidine HCl (CMH) to determine superoxide levels. Representative EPR waveforms are shown (C). Absolute levels of superoxide generation were then determined as nmols superoxide generated/min/mg protein (D). Reducing p47^{phox} protein levels significantly reduces the OGD-mediated increase in superoxide. Values are presented as mean ± S.E from 4 independent experiments using 24 pooled slices per experiment. *p<0.05 vs. uninfected no OGD, †p<0.05 vs. OGD exposed untransduced slices.

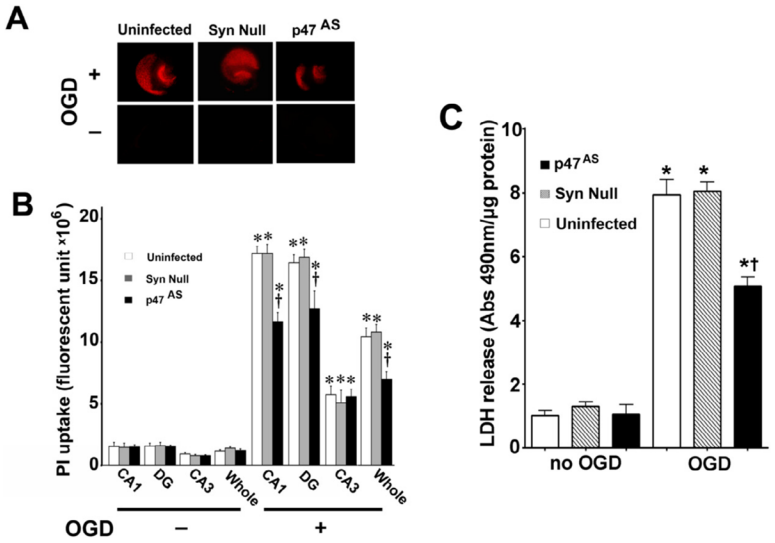

Figure 6. Targeted decreases in p47^{phox} expression in neuronal cells attenuates neuronal cell death in rat hippocampal slice cultures

Rat hippocampal slice cultures were transduced with the AAV-SYN-1-p47^{phox}AS, an AAV-SYN-1null construct, or were untransduced. After 7 days slices were exposed to OGD and the effect on PI uptake (A & B) and LDH release (C) was determined. Representative images are shown. Decreasing p47^{phox} expression reduces PI uptake in the whole slice as well as in the CA1 and DG regions but not in the CA3 (B). Similarly, Decreasing p47^{phox} expression reduces the OGD-mediated increases in LDH release (C). Values are presented as mean ± S.E from 4 independent experiments using 24 pooled slices per experiment. *p<0.05 vs. uninfected no OGD, †p<0.05 vs. OGD exposed untransduced slices.

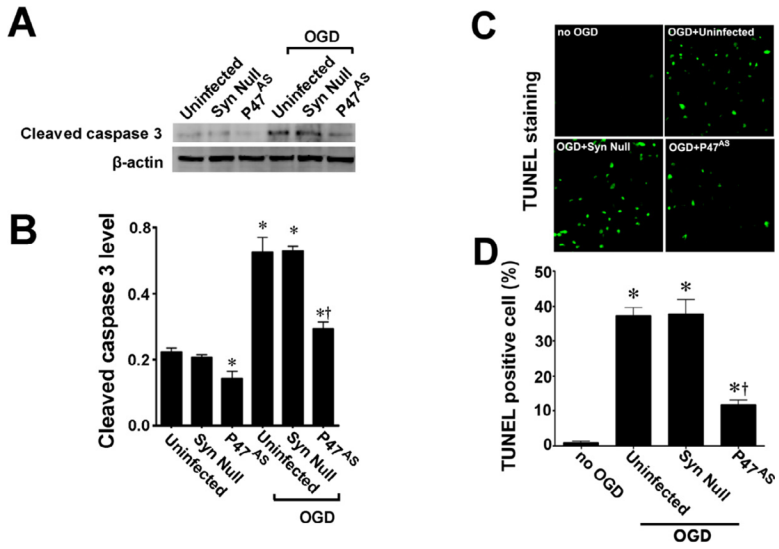

Figure 7. Targeted decreases in p47^{phox} expression in neuronal cells attenuates apoptotic cell death in rat hippocampal slice cultures

Rat hippocampal slice cultures were transduced with the AAV-SYN-1-p47^{phox}AS, an AAV-SYN-1null construct, or were untransduced. After 7 days slices were exposed to OGD and the effect on cleaved caspase-3 (A & B), and TUNEL positive nuclei (C & D) determined. Representative images are shown. Decreasing p47^{phox} expression reduces the OGD-mediated increases in cleaved caspase-3 (B) and the increase in TUNEL positive nuclei (D). Values are presented as mean ± S.E from 4 independent experiments using 24 pooled slices per experiment. *p<0.05 vs. uninfected no OGD, †p<0.05 vs. OGD exposed untransduced slices.

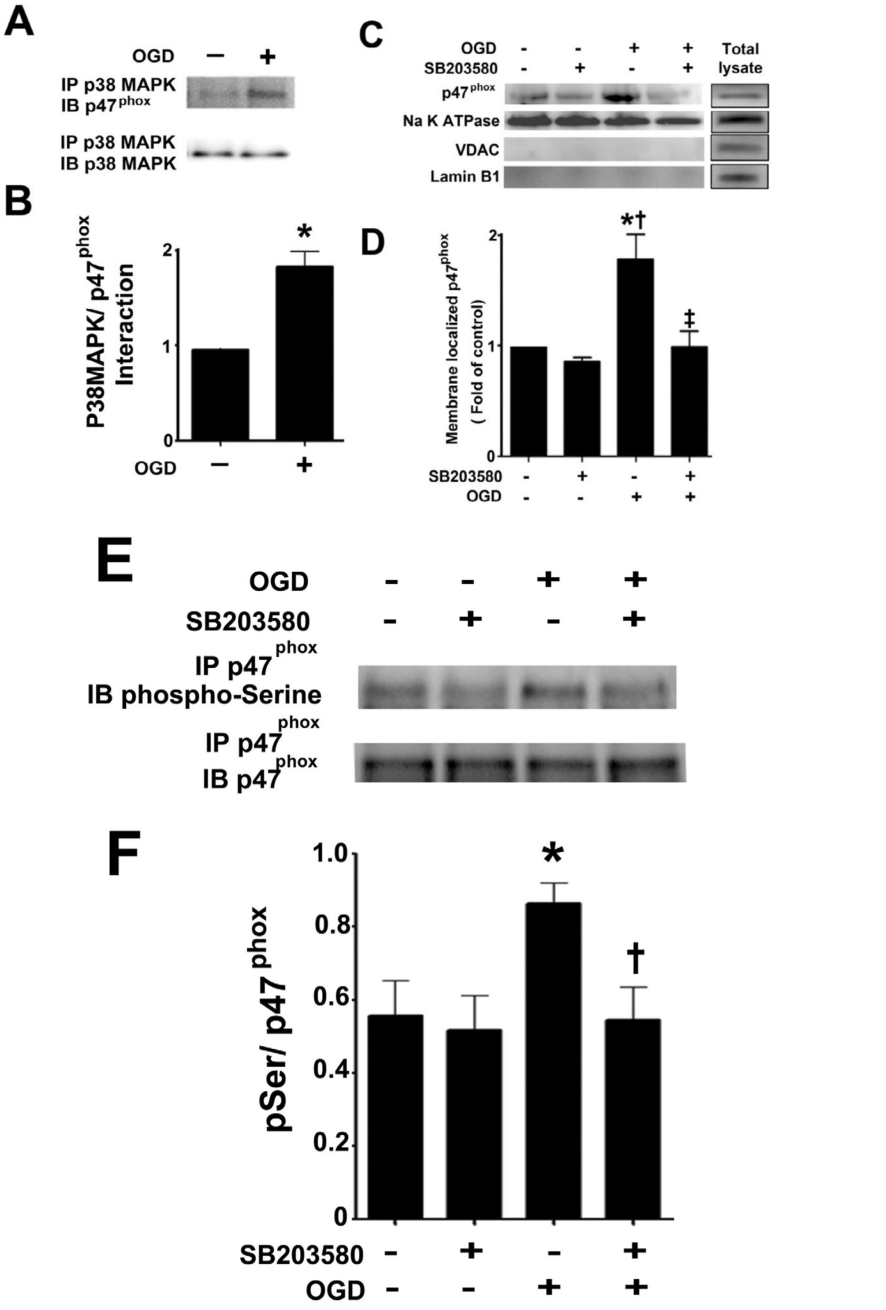

Figure 8. Oxygen glucose deprivation increases the p38MAP kinase mediated phosphorylation of p47phox

Rat hippocampal slice cultures were exposed to OGD then harvested 4h later and subjected to immunoprecipitation/Western blotting to determine the effect on the interaction of p38MAPK with p47phox (A & B). The effect of the p38MAPK inhibitor, SB203580 (50μM, 2h prior to OGD) on the OGD-mediated increase in plasma membrane translocation of p47phox 4h after OGD was also determined (C & D) as well as the effect on phospho-serine p47phox (E & F). Representative images are shown (A, C, E). OGD increases the interaction of p38MAPK with p47phox while both the OGD-mediated increases in p47phox membrane translocation and phospho-serine levels are attenuated by p38MAPK inhibition. Values are

presented as mean ± S.E from 4 independent experiments using 24 pooled slices per experiment. *p<0.05 vs. no OGD, †p<0.05 vs. OGD alone.

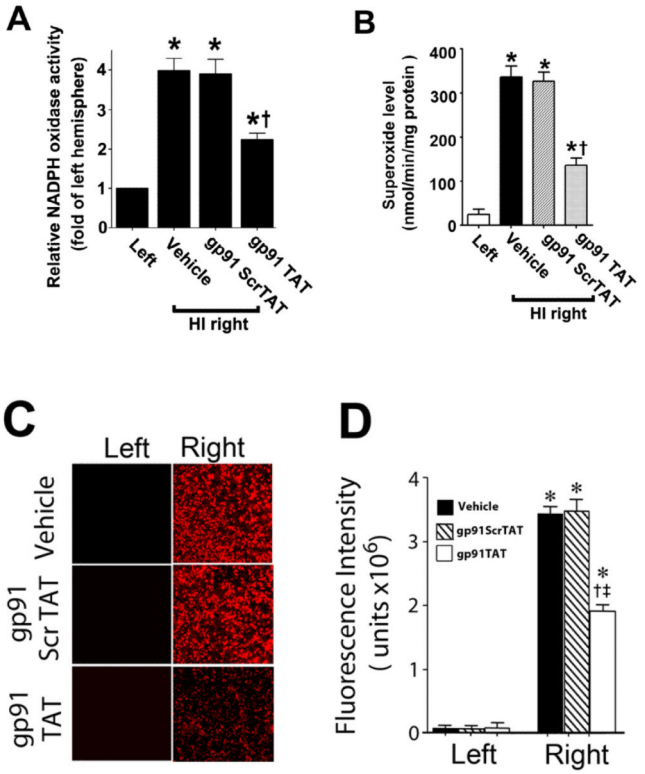

Figure 9. gp91ds-tat treatment attenuates NADPH oxidase activity and superoxide generation in the neonatal rat brain exposed to hypoxia-ischemia

P7 neonatal rats were pre-treated with gp91ds-tat, the scrambled control peptide, or vehicle then exposed to HI. Two hours after HI, NADPH oxidase activity (A) was determined in the left and right hemispheres of the brain. Superoxide levels were also determined using both EPR (B) and DHE oxidation (C & D). There is a significant increase in both NADPH oxidase activity and superoxide levels in the right hemisphere of the neonatal brain that is attenuated by gp91ds-tat, but not the scrambled peptide. Values are presented as mean ± S.D. from 5–6 animals per group. *p<0.05 vs. left hemisphere, †p<0.05 vs. HI + vehicle.

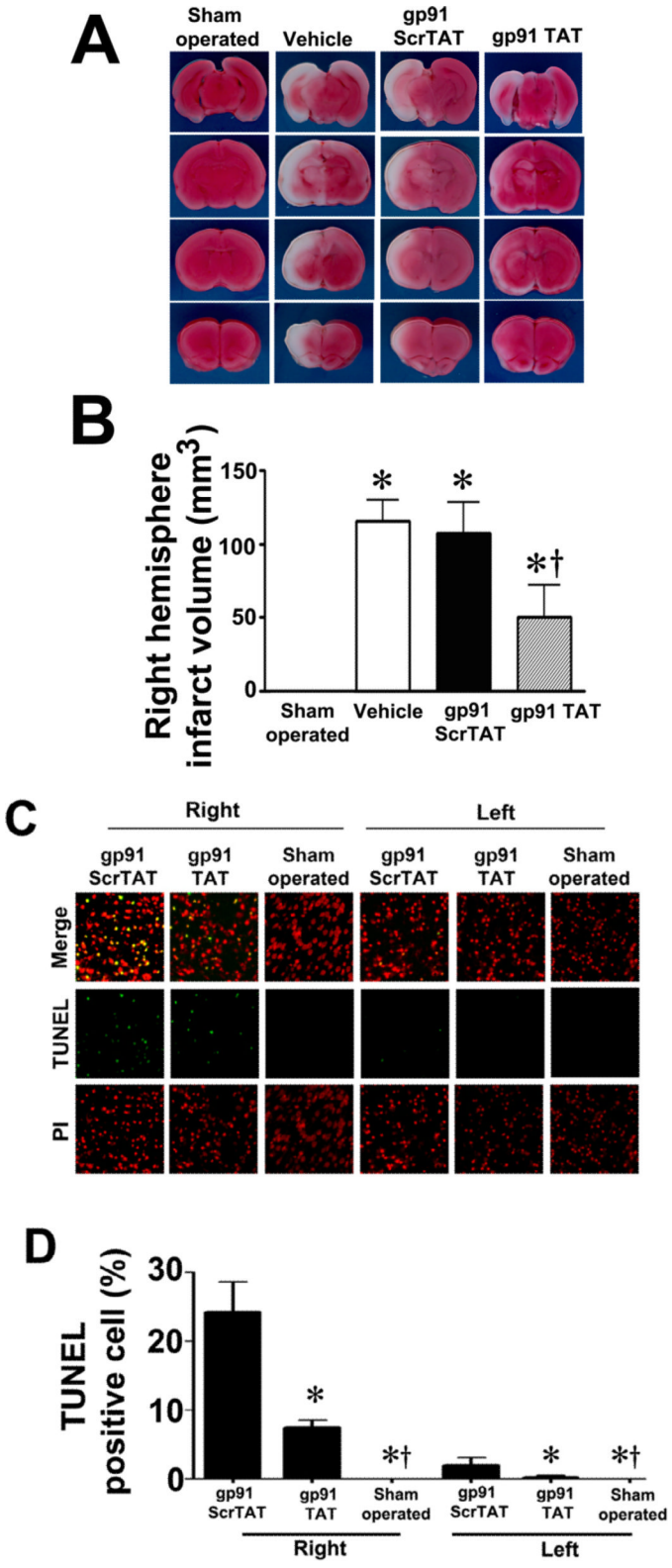

Figure 10. gp91ds-tat treatment attenuates neuronal injury in the neonatal rat brain exposed to hypoxia-ischemia

P7 neonatal rats were pre-treated with gp91dstat, the scrambled control peptide, or vehicle then exposed to HI. Twenty-four hours after HI the brains were removed, sectioned and subjected to TTC staining to determine the infarct volume in the right hemisphere. Representative TTC stained sections are shown (A). The HI-mediated increase in infract volume is attenuated by gp91ds-tat but not the scrambled peptide (B). TUNEL staining was also carried out 24h post-HI to determine the affect on apoptosis in the neonatal brain. Sections were counterstained with PI (red) and representative images are shown (C). Quantitation of TUNEL positive cells shows that gp91ds-tat, but not the scrambled peptide, attenuates the increase in apoptosis in the right hemisphere by HI (D). Values are presented as mean ± S.D. from 6 animals per group. *$p<0.05$ vs. left hemisphere, †$p<0.05$ vs. HI + vehicle.

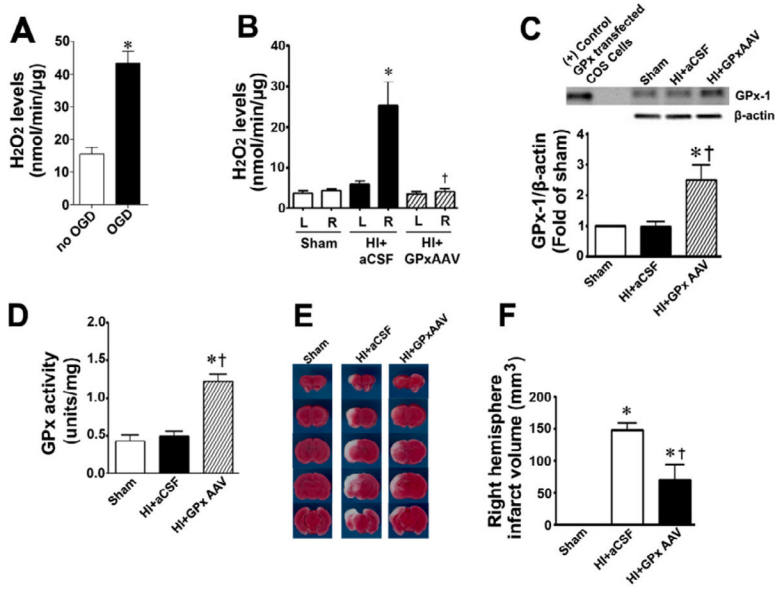

Figure 11. Scavenging H_2O_2 attenuates neuronal injury in the neonatal rat brain exposed to hypoxia-ischemia

Amplex Red assays demonstrated that H_2O_2 levels were significantly increased in hippocampal slice cultures exposed to OGD (A) and in the hippocampi of neonatal rats exposed to HI at P8 (B). The delivery of AAV GPx-1 significantly increased GPx-1 protein (C) and activity (D) in the hippocampus of the neonatal rat and significantly reduced H_2O_2 levels after exposure to HI (B). Twenty-four hours after HI the brains were removed, sectioned and subjected to TTC staining to determine the infarct volume in the right hemisphere. Representative TTC stained sections are shown (E). The HI-mediated increase in infract volume in the right hemisphere is significantly attenuated by the over-expression of GPx-1 (F). Values are presented as mean ± S.E. from 4 independent experiments using 24 pooled slices per experiment and as mean ± S.D. for 6 animals per group. In the slice cultures *p<0.05 vs. no OGD; in the rat brain *p<0.05 vs. sham, †p<0.05 vs. HI + artificial (a) CSF.